electronics

MDPI

Article

Two-Stage Combining and Beamforming Scheme for Multi-Pair Users FDD Massive MIMO Relay Systems

Dan Ge, Yunchao Song *, Tianbao Gao and Huibin Liang

College of Electronic and Optical Engineering & College of Flexible Electronics (Future Technology), Nanjing University of Posts and Telecommunications, Nanjing 210023, China; gedan@njupt.edu.cn (D.G.); 2018020231@njupt.edu.cn (T.G.); 2021020305@njupt.edu.cn (H.L.)

* Correspondence: songyc@njupt.edu.cn

Abstract

In this study, we consider multi-pair user frequency division duplexing massive MIMO relay systems and design a two-stage combining and beamforming (TSCB) scheme based on statistical channel state information (S-CSI). By leveraging S-CSI to co-design the pre-combining matrix and the pre-beamforming matrix, the scheme reduces the equivalent channel matrix dimensions, thereby cutting the pilot overhead. In the first stage, the two matrices are constructed through a selection of beams from a discrete Fourier transform codebook and mathematically cast as a multivariate optimization problem. An alternative optimization algorithm is proposed by splitting it into three sub-problems. The first two are 0–1 integer programming problems solved by iterative beam selection, while the third is a convex problem that is solved using a convex optimization algorithm. In the second stage, the reduced-dimension equivalent matrices are then estimated with low overhead, and a digital precoding matrix is then designed using zero-forcing algorithms. Simulations confirm the TSCB scheme's superior ESE performance over that of existing methods.

Keywords: massive MIMO; beam selection; relay; two-stage combining and beamforming; FDD

1. Introduction

Massive multiple-input multiple-output (MIMO) has shown great potential in the evolution of 5G and the development of 6G wireless systems [1–5]. When integrated with relay technology, it significantly extends network coverage and enhances both the reliability and efficiency of communications, particularly for cell-edge users [6–11]. Initial studies on massive MIMO relay systems assume perfect instantaneous channel state information (I-CSI) [12–17]. Suraweera [12] and Chen [13] analyze one-way system performance. For two-way systems, Rahimi [14] focuses on power efficiency and Chen [15] analyzes full-duplex systems. Furthermore, Rezaei [16] investigates multi-way systems.

Perfect I-CSI acquisition in practice is impeded by channel estimation errors, quantization noise, and feedback latency due to intrinsic limitations of pilot-based transmission and feedback mechanisms [18,19]. To address these challenges, research on massive MIMO relay systems has shifted to time division duplex (TDD) communications, leveraging channel reciprocity for downlink CSI estimation, thus reducing pilot and feedback overhead [20–26]. Compared to TDD, frequency division duplexing (FDD) eliminates uplink–downlink handoff and improves efficiency for symmetric or delay-sensitive flows. Consequently, FDD remains widely deployed in current networks and is predominant in industry and academic

Check for updates

Academic Editors: Adão Silva, Yuanxi Cao, Meng Wang and Enlin Wang

Received: 8 December 2025
Revised: 5 January 2026
Accepted: 7 January 2026
Published: 10 January 2026

Copyright: © 2026 by the authors. Licensee MDPI, Basel, Switzerland. This article is an open access article distributed under the terms and conditions of the Creative Commons Attribution (CC BY) license.

research, making FDD-based massive MIMO relay systems highly relevant for evolving networks [27–29].

Nonetheless, non-reciprocal FDD in massive MIMO relay systems presents a substantial challenge, as the overhead associated with pilot transmission for I-CSI estimation becomes prohibitively high when scaling up the number of antennas. Consequently, minimizing pilot overhead is essential for widespread adoption. The angles of departure and arrival (AoDs/AoAs) of CSI in uplink and downlink channels maintain reciprocity. Therefore, statistical channel state information (S-CSI) can leverage the inherent angle reciprocity to achieve a significant reduction in channel estimation overhead, thereby enhancing system robustness, improving delay compensation, and optimizing resource efficiency [30–32]. A beamforming matrix is designed at the relay for the maximization of the sum rate, with exclusive reliance on S-CSI [30]. Subsequently, a design of a precoding matrix for a correlated multi-relay MIMO system is considered, and an iterative algorithm based on S-CSI is proposed [31].

Although S-CSI ensures robustness and reduces pilot overhead, its performance lags behind that of I-CSI. Subsequently, a two-stage beamforming (TSB) scheme, which is named joint spatial division and multiplexing (JSDM) [33], is introduced to reduce pilot overhead while maintaining effective spectral efficiency (ESE). In this scheme, users in the same group share nearly identical feature spaces. S-CSI is utilized to eliminate inter-group interference and reduce channel dimensionality. To fully exploit the spatial domain, Song [34] proposes a neighbor-based JSDM, which fixes JSDM's grouping flaws via AOD-based neighbor/non-neighbor classification. For scenarios where S-CSI is unknown, a TSB scheme based on combinatorial multi-armed bandit (CMAB) is proposed [35]. This scheme transforms the pre-beamforming matrix design problem into a CMAB problem, which is solved by a UCB algorithm.

Traditional TSB schemes do not consider the relay scenarios. When relays are introduced, channel coupling arises between the multiple access channel (MAC) and broadcast channel (BC) phases, necessitating joint optimization of combining and beamforming to enhance overall system performance. Consequently, we propose a two-stage combining and beamforming (TSCB) scheme under constraints of limited radio frequency (RF) chains and a limited number of pilots (NOPs). By utilizing S-CSI at the relay station (RS) to jointly design the pre-combining and pre-beamforming matrices in the first stage, dimension-reduced equivalent channel matrices, namely instantaneous equivalent channel state information (IE-CSI) for the MAC and BC phases, can be obtained. By estimating the IE-CSI, a digital precoding matrix is designed in the second stage. The comparison of key features between the proposed scheme and existing works is shown in Table 1, and the main contributions are as follows:

- A novel TSCB scheme is introduced in a multi-pair-user FDD massive MIMO system to reduce the pilot overhead, thereby improving ESE. In the first stage, by using the S-CSI at the RS, we optimize the pre-combining matrix and pre-beamforming matrix jointly. In the second stage, due to the reduction in the dimensions of the IE-CSI after pre-combining and pre-beamforming, the IE-CSI can be estimated with lower pilot overhead. Subsequently, the ZF strategy is employed in the design of the digital precoding matrix to reduce multi-user interference, resulting in a higher ESE.
- The design of the pre-combining and pre-beamforming matrices is cast as a multivariate optimization task that involves 0-1 integer constraints. Considering the one-ring channel model and leveraging its intrinsic sparsity, the two matrices are designed by choosing beams from a discrete Fourier transform (DFT) codebook to reduce the implementation complexity with only the S-CSI known at the RS, thereby minimizing design and implementation complexity. The maximization of the system's receiving

energy, therefore, constitutes the objective function. Accounting for the practical limitations of RF chains and pilot overhead, we finally formulate the design problem into a form of multivariate optimization subject to 0-1 integer constraints.

- By an alternating optimization (AO) algorithm, the design of the pre-beamforming and pre-combining matrices is addressed, which targets improvements in the ESE. The design problem is broken down into three distinct sub-problems to be tackled by the AO algorithm. The first and second ones focus on obtaining the pre-beamforming and pre-combining matrices, which are recast as 0–1 integer programming problems. These problems are then solved by the proposed iterative beamforming selection (I-BS) and iterative combining selection (I-CS) algorithms. The third sub-problem involves an intermediate parameter matrix, which is a convex sub-problem, and a convex optimization is utilized to obtain the intermediate parameter matrix.

Table 1. Comparison of key features between proposed schemes.

Scheme	Assumption	Relay	Limited RF Chains	Limited NOP	Based on DFT
Digital [15]	I-CSI	Yes	Yes	No	No
Digital [31]	S-CSI	Yes	No	No	No
JSDM [33]	S-CSI	No	No	No	No
N-JSDM [34]	S-CSI	No	No	No	Yes
TSCB-proposed	S-CSI	Yes	Yes	Yes	Yes

We use boldface uppercase letters $\mathbf{A}$ for matrices and boldface lowercase letters $\mathbf{a}$ for vectors. Standard operations are denoted as follows: transpose as $[\cdot]^T$, Hermitian transpose as $[\cdot]^H$, conjugate as $[\cdot]^*$, trace as $\mathrm{tr}(\cdot)$, and Frobenius norm operators as $\|\cdot\|_F$. Meanwhile, $\mathbb{E}\{\cdot\}$ represents the expectation operator. We denote by the a_{mn}-th element of $\mathbf{A}$ and, by $\mathbf{a}_l$, its l-th column. A vector $\mathbf{a}_l \sim \mathcal{CN}(\mathbf{0}, \mathbf{R}_l)$ is a Gaussian variable with a zero mean and covariance matrix $\mathbf{R}_l$.

2. Preliminary

2.1. System Model and Channel Model

A relay-based half-duplex FDD massive MIMO system serving K user-pairs (UPs) is considered, as depicted in Figure 1. There are no direct links from the source users (SUs) to the destination users (DUs). The k-th SU, referred to as S_k, and the k-th DU, referred to as D_k, are equipped with one antenna and communicate exclusively via the RS equipped with M antennas. During the MAC phase, the SUs transmit information to the RS, while during the BC phase, the RS sends the processed signals to all DUs. The RS is configured with L_{RF} RF chains on both the reception and transmission sides. Upon detecting signals during the MAC phase, the RS employs a TSCB scheme to process them, subsequently broadcasting the refined signals in the BC phase.

We represent the channel vector from the source S_k to the RS as $\mathbf{h}_k \sim \mathcal{CN}(\mathbf{0}, \mathbf{R}_{S_k})$, and the channel vector from RS to D_k as $\mathbf{g}_k^H \sim \mathcal{CN}(\mathbf{0}, \mathbf{R}_{D_k})$, where $\mathbf{R}_{S_k} \in \mathbb{C}^{M\times M}$ and $\mathbf{R}_{D_k} \in \mathbb{C}^{M\times M}$ are the channel covariance matrices (CCMs) between the k-th UPs and the RS. Accordingly, the receiving signal at the RS is mathematically modeled as

$$\mathbf{y}_R = \sum_{k=1}^{K} \mathbf{h}_k x_{S_k} + \mathbf{n}_R = \mathbf{H}\mathbf{x}_S + \mathbf{n}_R, \tag{1}$$

where $\mathbf{H} = [\mathbf{h}_1, \mathbf{h}_2, \cdots, \mathbf{h}_K] \in \mathbb{C}^{M \times K}$ and $\mathbf{x}_S = [x_{S_1}, \cdots, x_{S_K}]^H \in \mathbb{C}^{K \times 1}$. $\mathbf{n}_R \sim \mathcal{CN}(0, \mathbf{I}_M)$ is the additive white Gaussian noise (AWGN).

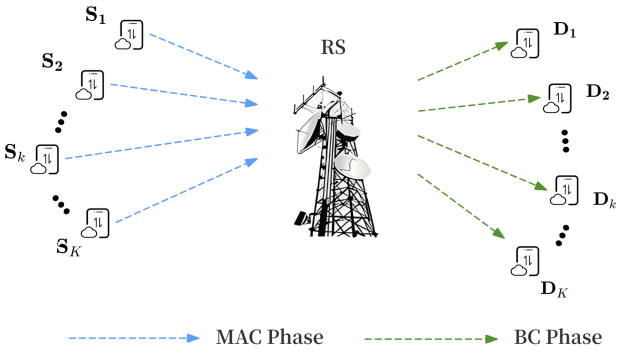


Figure 1. The system model.

Next, in the TSCB scheme depicted in Figure 2, an analog pre-combining matrix $\mathbf{B}_S^H$ and an analog pre-beamforming matrix $\mathbf{B}_D$ are designed for the RS in the first stage for the MAC and BC phases. Then, the digital precoding matrices $\mathbf{F}_1$ and $\mathbf{F}_2\mathbf{P}$ are further applied for the MAC and BC phases, respectively, in the second stage. Here, $\mathbf{P}$ is a shift matrix employed to recover the UPs. Therefore, the RS can process the received signal with $\mathbf{B}_D\mathbf{F}_2\mathbf{P}\mathbf{F}_1\mathbf{B}_S^H$, and the processed signal vector can be described as

$$\mathbf{x}_R = \mathbf{B}_D\mathbf{F}\mathbf{B}_S^H\mathbf{y}_R, \tag{2}$$

where $\mathbf{F} = \mathbf{F}_2\mathbf{P}\mathbf{F}_1$.

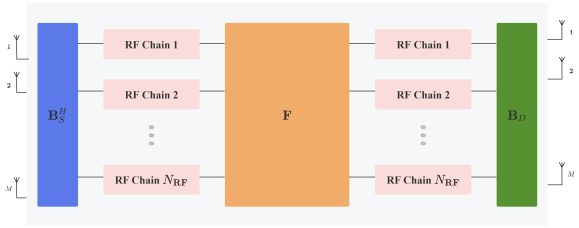


Figure 2. The proposed TSCB scheme.

Finally, $\mathbf{x}_R$ is broadcast from RS to all DUs in the BC phase. We can denote by $\mathbf{y}_D \in \mathbb{C}^{K \times 1}$ the received signal vector of all DUs, given as

$$\mathbf{y}_D = \underbrace{\mathbf{G}^H\mathbf{B}_D\mathbf{F}_2\mathbf{P}\mathbf{F}_1\mathbf{B}_S^H\mathbf{H}\mathbf{x}_S}_{signal} + \underbrace{\mathbf{G}^H\mathbf{B}_D\mathbf{F}_2\mathbf{P}\mathbf{F}_1\mathbf{B}_S^H\mathbf{n}_R + \mathbf{n}_D}_{noise}, \tag{3}$$

where $\mathbf{G}^H = [\mathbf{g}_1, \mathbf{g}_2, \cdots, \mathbf{g}_K]^H \in \mathbb{C}^{K \times M}$ and $\mathbf{n}_D \in \mathbb{C}^{K \times 1} \sim \mathcal{CN}(0, \mathbf{I}_K)$ is the AWGN.

The S-CSI is assumed to be available at the RS. For the k-th UP (S_k - D_k), the scattering radii in the MAC and BC phases are denoted as r_{S_k} and r_{D_k}, the central angles as θ_{S_k} and θ_{D_k}, and the angular spreads (ASs) as Δ_{S_k} and Δ_{D_k} respectively, where $k = 1, 2, \ldots, K$. Consequently, the CCMs $\mathbf{R}_{S_k}$ and $\mathbf{R}_{D_k}$ can be described as

$$\mathbf{R}_{S_k} = \frac{1}{2\Delta_{S_k}} \int_{\theta_{S_k}-\Delta_{S_k}}^{\theta_{S_k}+\Delta_{S_k}} \gamma(\theta)\mathbf{a}^*(\theta)\mathbf{a}^T(\theta)d\theta, \tag{4}$$

$$\mathbf{R}_{D_k} = \frac{1}{2\Delta_{D_k}} \int_{\theta_{D_k}-\Delta_{D_k}}^{\theta_{D_k}+\Delta_{D_k}} \gamma(\theta)\mathbf{a}^*(\theta)\mathbf{a}^T(\theta)d\theta, \tag{5}$$

where $\mathbf{a}(\theta)$ is the array steering vector, the m-th element of which is $\frac{1}{M}e^{i2\pi\frac{d}{\lambda_c}(m-1)\sin\theta}$. The carrier wavelength is λ_c. Let d be the antenna spacing for the ULA. $\gamma(\theta)$ represents the power azimuth spectrum of the channel with the property that $\int_{\theta_{S_k}-\Delta_{S_k}}^{\theta_{S_k}+\Delta_{S_k}}\gamma(\theta)d\theta = \int_{\theta_{D_k}-\Delta_{D_k}}^{\theta_{D_k}+\Delta_{D_k}}\gamma(\theta)d\theta = 1$. For randomly distributed users, we simplify the processing by reordering the azimuths of the UPs in ascending order.

The channel vectors $\mathbf{h}_k$ and $\mathbf{g}_k$ can be further written in the Karhunen–Loeve form as

$$\mathbf{h}_k = \mathbf{R}_{S_k}^{1/2}\mathbf{z}_{S_k}, \tag{6}$$

$$\mathbf{g}_k = \mathbf{R}_{D_k}^{1/2}\mathbf{z}_{D_k}, \tag{7}$$

where $\mathbf{z}_{S_k} \sim \mathcal{CN}(0,\mathbf{I})$ and $\mathbf{z}_{D_k} \sim \mathcal{CN}(0,\mathbf{I})$ represent the small-scale fading.

2.2. The Equivalent Channel Matrix and Matrix Sparsity

The inherent absence of channel reciprocity in FDD massive MIMO complicates the design. To overcome this challenge, a TSCB scheme is introduced to reduce the dimension of the IE-CSI, thereby reducing pilot overhead and feedback.

As illustrated in Figure 2, the IE-CSI consists of a pre-combining matrix $\mathbf{B}_S^H \in \mathbb{C}^{L_S\times M}$ and a pre-beamforming matrix $\mathbf{B}_D \in \mathbb{C}^{M\times L_D}$, used for the MAC and BC phases, respectively. We now provide a brief description of the channel estimation process for IE-CSI as follows. Note that

$$\mathbf{Y}_R^H = \mathbf{B}_S^H\mathbf{H}\mathbf{X}_S + \bar{\mathbf{N}}_R, \tag{8}$$

$$\mathbf{Y}_D^H = \mathbf{G}^H\mathbf{B}_D\mathbf{X}_R + \mathbf{N}_D, \tag{9}$$

where $\mathbf{X}_S$ and $\mathbf{X}_R$ are the pilot matrices. $\mathbf{Y}_R$ is the received signal after pre-combining at the RS and $\bar{\mathbf{N}}_R = \mathbf{B}_S^H\mathbf{N}_R$. $\mathbf{Y}_D$ and $\mathbf{N}_D$ are similar matrices at the DUs.

Further letting $\mathbf{B}_D = [\mathbf{b}_{D_1}, \mathbf{b}_{D_2}, \cdots, \mathbf{b}_{D_{L_D}}]$ and $\mathbf{B}_S^H = [\mathbf{b}_{S_1}, \mathbf{b}_{S_2}, \cdots, \mathbf{b}_{S_{L_S}}]^H$, the IE-CSI $\bar{\mathbf{G}} = \mathbf{G}^H\mathbf{B}_D \in \mathbb{C}^{K\times L_D}$ and $\bar{\mathbf{H}} = \mathbf{B}_S^H\mathbf{H} \in \mathbb{C}^{L_S\times K}$ for the two phases are given by

$$\mathbf{G}^H\mathbf{B}_D = \begin{bmatrix} \mathbf{g}_1^H\mathbf{b}_{D_1} & \mathbf{g}_1^H\mathbf{b}_{D_2} & \cdots & \mathbf{g}_1^H\mathbf{b}_{D_{L_D}} \\ \mathbf{g}_2^H\mathbf{b}_{D_1} & \mathbf{g}_2^H\mathbf{b}_{D_2} & \cdots & \mathbf{g}_2^H\mathbf{b}_{D_{L_D}} \\ \vdots & \vdots & \ddots & \vdots \\ \mathbf{g}_K^H\mathbf{b}_{D_1} & \mathbf{g}_K^H\mathbf{b}_{D_2} & \cdots & \mathbf{g}_K^H\mathbf{b}_{D_{L_D}} \end{bmatrix}, \tag{10}$$

$$\mathbf{B}_S^H\mathbf{H} = \begin{bmatrix} \mathbf{b}_{S_1}^H\mathbf{h}_1 & \mathbf{b}_{S_1}^H\mathbf{h}_2 & \cdots & \mathbf{b}_{S_1}^H\mathbf{h}_K \\ \mathbf{b}_{S_2}^H\mathbf{h}_1 & \mathbf{b}_{S_2}^H\mathbf{h}_2 & \cdots & \mathbf{b}_{S_2}^H\mathbf{h}_K \\ \vdots & \vdots & \ddots & \vdots \\ \mathbf{b}_{S_{L_S}}^H\mathbf{h}_1 & \mathbf{b}_{S_{L_S}}^H\mathbf{h}_2 & \cdots & \mathbf{b}_{S_{L_S}}^H\mathbf{h}_K \end{bmatrix}. \tag{11}$$

By designing $\mathbf{B}_D$ and $\mathbf{B}_S^H$, we can induce sparsity in the first stage, resulting in $\bar{\mathbf{G}}$ and $\bar{\mathbf{H}}$ having some zero entries. Leveraging the inherent properties, the equivalent channel vectors $\bar{\mathbf{g}}_k$ and $\bar{\mathbf{h}}_k$ can be expressed as

$$\bar{\mathbf{g}}_k = [\cdots, 0, \mathbf{g}_k^H\mathbf{b}_{D_p}, \cdots, \mathbf{g}_k^H\mathbf{b}_{D_q}, 0, \cdots], \tag{12}$$

$$\bar{\mathbf{h}}_k = [\cdots, 0, \mathbf{h}_k^H\mathbf{b}_{S_p}, \cdots, \mathbf{h}_k^H\mathbf{b}_{S_q}, 0, \cdots]^H. \tag{13}$$

Note that $\bar{\mathbf{G}}$ and $\bar{\mathbf{H}}$ are banded matrices, and we design the pilot matrices for the two phases to have a circular structure as

$$\mathbf{X}_R = [\mathbf{x}_{R_1}, \mathbf{x}_{R_2}, \cdots, \mathbf{x}_{\mu_R}, \mathbf{x}_{R_1}, \cdots]^H, \tag{14}$$

$$\mathbf{X}_S = [\mathbf{x}_{S_1}, \mathbf{x}_{S_2}, \cdots, \mathbf{x}_{\mu_S}, \mathbf{x}_{S_1}, \cdots]^H, \tag{15}$$

where $\mathbf{X}_R$ and $\mathbf{X}_S$ have the dimensions $L_D \times \mathcal{L}_D$ and $K \times \mathcal{L}_S$, respectively, constructed from the orthogonal pilot vectors $\mathbf{x}_{R_l}$ and $\mathbf{x}_{S_l}$. $\mathcal{L}_D$ and $\mathcal{L}_S$ denote the training length, respectively. The necessity to estimate only the non-zero elements significantly reduces the pilot overhead. The minimum training length of $\mathcal{L}_D$ and $\mathcal{L}_S$ are

$$\mathcal{L}_{D_0} = \max_k d_{D_k}, \tag{16}$$

$$\mathcal{L}_{S_0} = \max_l d_{S_l}, \tag{17}$$

where d_{D_k} is the number of non-zero elements of the k-th row of $\bar{\mathbf{G}}$ and d_{S_l} denotes the number of non-zero elements of the l-th row of $\bar{\mathbf{H}}$. Since $\mathbf{X}_R$ and $\mathbf{X}_S$ have circular forms, the minimum NOPs are denoted by μ_S and μ_R in the MAC and BC phases, respectively. Therefore, μ_R should be no smaller than the minimum training length $\mathcal{L}_{D_0}$, and similarly, μ_S should be no smaller than $\mathcal{L}_{S_0}$. The above formulation assumes perfect IE-CSI at the RS, enabled by state-of-the-art channel estimation techniques.

3. Two-Stage Combining and Beamforming Scheme

3.1. The Design of Pre-Combining and Pre-Beamforming Matrices

With S-CSI available at the RS, we can devise $\mathbf{B}_D$ and $\mathbf{B}_S^H$. Furthermore, the dimensionality of the IE-CSI can be substantially reduced by estimating its non-zero entries during the two phases.

To sparsify the IE-CSI $\bar{\mathbf{g}}_k = \mathbf{g}_k^H \mathbf{B}_D$ and $\bar{\mathbf{h}}_k = \mathbf{B}_S^H \mathbf{h}_k$, we should design the two matrices satisfying the following constraints:

$$\mathbf{g}_k^H \mathbf{b}_{D_l} = 0, \tag{18}$$

$$\mathbf{b}_{S_l}^H \mathbf{h}_k = 0, \tag{19}$$

where $\mathbf{b}_{D_l}$ and $\mathbf{b}_{S_l}$ are the l-th columns of $\mathbf{B}_D$ and $\mathbf{B}_S$, respectively. Substituting (6) and (7) into (18) and (19), respectively, we can obtain

$$\mathbf{z}_{D_k}^H \mathbf{R}_{D_k}^{\frac{1}{2}} \mathbf{b}_{D_l} = 0, \tag{20}$$

$$\mathbf{b}_{S_l}^H \mathbf{R}_{S_k}^{\frac{1}{2}} \mathbf{z}_{S_k} = 0, \tag{21}$$

where $\mathbf{z}_{D_k}$ and $\mathbf{z}_{S_k}$ represent the small-scaling fading. Since $\mathbf{z}_{D_k}$ and $\mathbf{z}_{S_k}$ are random variables, (20) and (21) are, respectively, equivalent to

$$\mathbf{R}_{D_k}^{\frac{1}{2}} \mathbf{b}_{D_l} = 0, \tag{22}$$

$$\mathbf{b}_{S_l}^H \mathbf{R}_{S_k}^{\frac{1}{2}} = 0. \tag{23}$$

By leveraging the inherent sparsity of the one-ring channel, the CCMs $\mathbf{R}_{D_k}$ and $\mathbf{R}_{S_k}$ can be sparsified by DFT matrices. To this end, we proceed by co-designing $\mathbf{B}_D$ and $\mathbf{B}_S^H$ through a DFT codebook, where the DFT codebook $\mathcal{U}$ is given as

$$\mathcal{U} = \{\mathbf{u}_m | \mathbf{u}(m-1) = \mathbf{u}(z_{m-1}), m \in \mathcal{M} = \{1, \cdots, M\}\}, \tag{24}$$

$z_{m-1} = \sin\Phi_{m-1}$, and $\mathbf{u}(z_{m-1})$ is a vector with the n-th ($n = 1, \ldots, M$) element being $\frac{1}{\sqrt{M}} e^{-i\pi(n-1)z_{m-1}}$.

3.2. Problem Formulation with Limited RF Chains and Pilots

To reduce the implementation costs, computational complexity, and energy consumption, the number of RF chains is set to be much lower than the number of antennas. Furthermore, to reduce the pilot overhead for IE-CSI estimation, limited pilots should be considered. We maximize the received signal energy $\mathbb{E}\|\mathbf{G}^H\mathbf{B}_D\mathbf{F}_2\mathbf{P}\mathbf{F}_1\mathbf{B}_S^H\mathbf{H}\|_F^2$ to maximize the ESE, with the key constraints: (1) RF chain limitation: the numbers of columns in both $\mathbf{B}_S$ and $\mathbf{B}_D$ do not exceed the available RF chains L_{RF}; (2) pilot overhead limitation: the NOPs μ_R and μ_S for the two phases should not be larger than the maximum allowable number N; (3) codebook constraint: all column vectors $\mathbf{b}_{D_l}$ and $\mathbf{b}_{S_l}$ are selected from the codebook $\mathcal{U}$. Based on the above constraints, we formulate the problem of designing two matrices in the first stage as

$$\mathcal{P}_1: \quad \max_{\mathbf{B}_D, \mathbf{B}_S, \mathbf{F}} \mathbb{E}\|\mathbf{G}^H\mathbf{B}_D\mathbf{F}\mathbf{B}_S^H\mathbf{H}\|_F^2 \tag{25a}$$

$$s.t. \quad col(\mathbf{B}_D) \le L_{RF}, \tag{25b}$$

$$col(\mathbf{B}_S) \le L_{RF}, \tag{25c}$$

$$\mu_R \le N, \mu_S \le N, \tag{25d}$$

$$\mathbf{b}_{D_l} \in \mathcal{U}, \mathbf{b}_{S_l} \in \mathcal{U}, \tag{25e}$$

$$tr(\mathbf{F}^H\mathbf{F}) \le P, \tag{25f}$$

where $\mathbf{F} = \mathbf{F}_2\mathbf{P}\mathbf{F}_1$.

With S-CSI known at the RS, applying (6) and (7) to $\mathcal{P}_1$, the function in (25a) can be transformed to

$$\mathbb{E}\|\mathbf{G}^H\mathbf{B}_D\mathbf{F}\mathbf{B}_S^H\mathbf{H}\|_F^2 \tag{26a}$$

$$= \mathbb{E}\{tr(\mathbf{B}_D^H\sum_{i=1}^{K}\mathbf{g}_i\mathbf{g}_i^H\mathbf{B}_D\mathbf{F}\mathbf{B}_S^H\sum_{j=1}^{K}\mathbf{h}_j\mathbf{h}_j^H\mathbf{B}_S\mathbf{F}^H)\} \tag{26b}$$

$$= tr(\mathbf{B}_D^H\sum_{i=1}^{K}\mathbf{R}_{D_i}\mathbf{B}_D \cdot \mathbf{F}\mathbf{B}_S^H\sum_{j=1}^{K}\mathbf{R}_{S_j}\mathbf{B}_S\mathbf{F}^H). \tag{26c}$$

Moreover, we define two matrices, $\mathbf{Q}_D$ and $\mathbf{Q}_S$, as follows:

$$q_{D_{k,l}} = \begin{cases} \|\mathbf{R}_{D_k}^{1/2}\mathbf{u}_l\|_2^2, & \|\mathbf{R}_{D_k}^{1/2}\mathbf{u}_l\|_2^2 > \xi, \\ 0, & \|\mathbf{R}_{D_k}^{1/2}\mathbf{u}_l\|_2^2 \le \xi, \end{cases} \tag{27}$$

$$q_{S_{k,l}} = \begin{cases} \|\mathbf{R}_{S_k}^{1/2}\mathbf{u}_l\|_2^2, & \|\mathbf{R}_{S_k}^{1/2}\mathbf{u}_l\|_2^2 > \xi, \\ 0, & \|\mathbf{R}_{S_k}^{1/2}\mathbf{u}_l\|_2^2 \le \xi, \end{cases} \tag{28}$$

where $q_{D_{k,l}}$ and $q_{S_{k,l}}$ correspond to the average energy of the k-th UP within the m-th DFT codeword and ξ is the energy threshold. We set $q_{D_{k,l}}$ ($q_{S_{k,l}}$) to zero when $\|\mathbf{R}_{D_k}^{1/2}\mathbf{u}_l\|_2^2$ $\left(\|\mathbf{R}_{S_k}^{1/2}\mathbf{u}_l\|_2^2\right)$ falls below the threshold ξ. This approximation helps to sparsify the IE-CSI.

Next, we define two index matrices, $\hat{\mathbf{Q}}_D$ and $\hat{\mathbf{Q}}_S$, to locate the non-zero elements of $\mathbf{Q}_D$ and $\mathbf{Q}_S$. Let $\hat{q}_{D_{k,l}}$ and $\hat{q}_{S_{k,l}}$ be the (k,l)-th elements of $\hat{\mathbf{Q}}_D$ and $\hat{\mathbf{Q}}_S$, respectively. Then,

$$\hat{q}_{D_{k,l}} = \begin{cases} 1, & q_{D_{k,l}} \text{is not zero}, \\ 0, & \text{otherwise}. \end{cases} \hat{q}_{S_{k,l}} = \begin{cases} 1, & q_{S_{k,l}} \text{is not zero}, \\ 0, & \text{otherwise}. \end{cases} \tag{29}$$

Finally, to describe the constraints (25b)–(25d), we define two beam-selected index vectors, $\mathbf{d}_D$ and $\mathbf{s}_S$, in the two phases as

$$\mathbf{d}_D = [d_1, d_2, \cdots, d_M]^T, \ \mathbf{s}_S = [s_1, s_2, \cdots, s_M]^T, \tag{30}$$

where s_l and d_l are used to indicate whether or not the l-th codeword in the codebook $\mathcal{U}$ is selected, and

$$d_l = \begin{cases} 1, & \mathbf{u}_l \text{ be selected}, \\ 0, & \mathbf{u}_l \text{ not be selected}, \end{cases} s_l = \begin{cases} 1, & \mathbf{u}_l \text{ be selected}, \\ 0, & \mathbf{u}_l \text{ not be selected}. \end{cases} \tag{31}$$

Denote by L_D and L_S the column numbers of $\mathbf{B}_D$ and $\mathbf{B}_S$, respectively. Then, we have $L_D = \sum_{l=1}^{M} d_l$ and $L_S = \sum_{l=1}^{M} s_l$, and (25b) and (25c) are transformed to

$$\sum_{l=1}^{M} d_l \leq L_{RF}, \tag{32}$$

$$\sum_{l=1}^{M} s_l \leq L_{RF}. \tag{33}$$

Simultaneously, the constraints of the minimum NOPs μ_R and μ_S in (25d) can be described using the index vectors $\mathbf{d}_D$ and $\mathbf{s}_S$ and the index matrices $\hat{\mathbf{Q}}_D$ and $\hat{\mathbf{Q}}_S$ as

$$\mu_R = \sum_{l=1}^{M} d_l \hat{q}_{D_{k,l}} \leq N, \tag{34}$$

$$\mu_S = \sum_{k=1}^{K} s_l \hat{q}_{S_{k,l}} \leq N. \tag{35}$$

From the above discussion, the problem $\mathcal{P}_1$ can be transformed to

$$\mathcal{P}_2 \quad \max_{\mathbf{B}_D, \mathbf{B}_S, \mathbf{F}} tr(\mathbf{B}_S^H \sum_{i=1}^{K} \mathbf{R}_{S_i} \mathbf{B}_S \cdot \mathbf{F}^H \mathbf{B}_D^H \sum_{j=1}^{K} \mathbf{R}_{D_j} \mathbf{B}_D \mathbf{F}) \tag{36a}$$

$$s.t. \quad \sum_{l=1}^{M} d_l \leq L_{RF}, \sum_{l=1}^{M} s_l \leq L_{RF} \tag{36b}$$

$$\sum_{l=1}^{M} d_l \hat{q}_{D_{k,l}} \leq N, \sum_{k=1}^{K} s_l \hat{q}_{S_{k,l}} \leq N, \tag{36c}$$

$$d_l = \{0,1\}, s_l = \{0,1\}, \tag{36d}$$

$$\mathbf{b}_{D_l} \in \mathcal{U}, \mathbf{b}_{S_l} \in \mathcal{U}, \tag{36e}$$

$$tr(\mathbf{F}^H \mathbf{F}) \leq P. \tag{36f}$$

The problem $\mathcal{P}_2$ involves three key variables: $\mathbf{B}_S$, $\mathbf{B}_D$, and $\mathbf{F}$. It should be noted that the matrix $\mathbf{F}$ is designed using the S-CSI, and it will be updated in the second stage using the IE-CSI. To solve $\mathcal{P}_2$, we propose an AO algorithm in this paper, which decomposes $\mathcal{P}_2$ into three sub-problems. The first sub-problem is to design $\mathbf{B}_D$, given $\mathbf{B}_S$ and $\mathbf{F}$. Let

$\mathbf{A}_S = \mathbf{F}\mathbf{B}_S^H \sum_{k'=1}^{K} \mathbf{R}_{S_k'} \mathbf{B}_S \mathbf{F}^H$, the i-th row and j-th column entry of which is $a_{S_{i,j}}$. Since $\mathbf{B}_D$ is formed by selecting beams from the DFT codebook, we have $\mathbf{b}_{D_n}^H \cdot \mathbf{b}_{D_{n'}} = 0$ for $n \neq n'$. Consequently, the first sub-problem is formulated as

$$\mathcal{P}_{3-1} \quad \max_{\mathbf{b}_{D_n}, d_l} \sum_{k=1}^{K} \sum_{n=1}^{L_D} a_{S_{n,n}} \|\mathbf{R}_{D_k}^{1/2} \mathbf{b}_{D_n}\|_2^2 \tag{37a}$$

$$s.t. \quad \sum_{l=1}^{M} d_l \leq L_{RF}, \tag{37b}$$

$$\sum_{l=1}^{M} d_l \bar{q}_{D_{k,l}} \leq N, \tag{37c}$$

$$d_l = \{0, 1\}, \tag{37d}$$

$$\mathbf{b}_{D_n} \subseteq \mathcal{U}. \tag{37e}$$

The problem $\mathcal{P}_{3-1}$ is a weighted 0–1 quadratic programming problem with quadratic constraint. To tackle this problem, we propose an I-BS scheme, which selects the optimal beam to construct $\mathbf{B}_D$ in each iteration. In the initial iteration, we select the l-th codeword $\mathbf{u}_l$ that maximizes (37a) to be the column b_{D_1}. For subsequent iterations, we consistently choose one unselected codeword that maximizes (37a). The iteration process terminates when either the iteration count $k = \sum_{l=1}^{M} d_l$ exceeds L_{RF} or $\mu_R = \max_k \sum_{l=1}^{M} d_l \hat{q}_{D_{k,l}}$ surpasses N. The process is detailed in Algorithm 1.

Algorithm 1: I-BS scheme

Input: $\mathbf{R}_{S_k}, \mathbf{R}_{D_k}, L_{RF}, N, \mathcal{U}, \mathbf{B}_S, \mathbf{F}$;
Output: $\mathbf{B}_D$;
Initialize $f^{(0)} = 0$, $\mathbf{S}^{(1)} = \mathbf{S}$, $d_l = 0$, $\mu_R = 0$; $k = 0$;
while $k \leq L_{RF}, \mu_R \leq N$ **do**
  for $l = 1, 2, \ldots, M$ **do**
    Set $d_l = 1$;
    Compute $f_l^{(k)} = \sum_{k=1}^{K} \sum_{n=1}^{L_D} a_{S_{n,n}} \|\mathbf{R}_{D_k}^{1/2} \mathbf{u}_l\|_2^2 \cdot d_l$;
  end
  Set $d_l = 1 \leftarrow$ Find $l = \arg_l \max f_l^{(k)}$;
  Set $\mathbf{b}_{D_n} = \mathbf{u}(l)$ for $d_l = 1$;
  Use (37c) to compute μ_R, ;
  Update unselected codebook $\mathcal{S}^{(k+1)}$;
  Set $k = k + 1$;
end
return $\mathbf{B}_D = [b_{D_1}, \cdots, b_{D_{L_D}}]$.

Similarly to the first sub-problem, the second sub-problem is to devise $\mathbf{B}_S$, given as $\mathbf{B}_D$ and $\mathbf{F}$. Let $\mathbf{A}_D = \mathbf{F}^H \mathbf{B}_D^H \sum_{k=1}^{K} \mathbf{R}_{D_k} \mathbf{B}_D \mathbf{F}$, i-th row and j-th column entry of which is $a_{D_{i,j}}$. The second sub-problem is thus formulated as

$$\mathcal{P}_{3-2} \quad \max_{\mathbf{b}_{S,n}, s_l} \sum_{k=1}^{K} \sum_{n=1}^{L_S} a_{D_{n,n}} \|\mathbf{R}_{S_k}^{1/2} \mathbf{b}_{S_n}\|_2^2 \tag{38a}$$

$$s.t. \quad \sum_{l=1}^{M} s_l \leq L_{RF}, \tag{38b}$$

$$\sum_{k=1}^{K} s_l \hat{q}_{S_{k,l}} \leq N, \tag{38c}$$

$$s_l = \{0, 1\}, \tag{38d}$$

$$\mathbf{b}_{S_n} \subseteq \mathcal{U}. \tag{38e}$$

Using a method similar to Algorithm 1, the problem $\mathcal{P}_{3-2}$ can be solved. The steps are detailed in Algorithm 2.

Algorithm 2: I-CS scheme

Input: $\mathbf{R}_{S_k}$, $\mathbf{R}_{D_k}$,L_{RF}, $N, \mathcal{U}$, $\mathbf{B}_D$, $\mathbf{F}$;
Output: $\mathbf{B}_S$;
Initialize $f^{(0)} = 0$, $\mathbf{S}^{(1)} = \mathbf{S}$, $s_l = 0$, $\mu_S = 0$; set k as the number of iterations;
while $k \leq L_{RF}, \mu_S \leq N$ **do**
  for $l = 1, 2, \ldots, M$ **do**
    Set $s_l = 1$;
    Compute $f_l^{(k)} = \sum_{k=1}^{K} \sum_{n=1}^{L_D} a_{S_{n,n}} \|\mathbf{R}_{S_k}^{1/2} \mathbf{u}_m\|_2^2 \cdot s_l$;
  end
  Set $s_l = 1 \leftarrow$ Find $l = \arg_l \max f_l^{(k)}$;
  Set $\mathbf{b}_{S_n} = \mathbf{u}(l)$ for $s_l = 1$;
  Compute μ_S, according to (38c);
  Update unselected codebook $\mathcal{S}^{(k+1)}$;
  Set $k = k + 1$;
end
return $\mathbf{B}_S = [b_{S_1}, \cdots, b_{S_{L_S}}]$.

The third sub-problem is to devise $\mathbf{F}$ given $\mathbf{B}_S$ and $\mathbf{B}_D$. Letting $\bar{\mathbf{A}}_S = \mathbf{B}_S^H \sum_{k'=1}^{K} \mathbf{R}_{S_{k'}} \mathbf{B}_S$ and $\bar{\mathbf{A}}_D = \mathbf{B}_D^H \sum_{k=1}^{K} \mathbf{R}_{D_k} \mathbf{B}_D$, the third sub-problem is formulated as

$$\mathcal{P}_{3-3} \quad \max_{\mathbf{F}} tr(\bar{\mathbf{A}}_S \mathbf{F}^H \bar{\mathbf{A}}_D \mathbf{F}) \tag{39a}$$

$$s.t. \ tr(\mathbf{F}^H \mathbf{F}) \leq P. \tag{39b}$$

By applying singular value decomposition (SVD) to $\mathbf{F}$ as $\mathbf{F} = \mathbf{U}_F \mathbf{\Sigma}_F \mathbf{V}_F^H$, and since $\bar{\mathbf{A}}_S = (\mathbf{R}_S^{\frac{1}{2}} \mathbf{B}_S)^H (\mathbf{R}_S^{\frac{1}{2}} \mathbf{B}_S)$ and $\bar{\mathbf{A}}_D = (\mathbf{R}_D^{\frac{1}{2}} \mathbf{B}_D)^H (\mathbf{R}_D^{\frac{1}{2}} \mathbf{B}_D)$, where $\mathbf{R}_S = \sum_{k'=1}^{K} \mathbf{R}_{S_{k'}}$ and $\mathbf{R}_D = \sum_{k=1}^{K} \mathbf{R}_{D_k}$, (39a) can be transformed into

$$tr(\bar{\mathbf{A}}_S \mathbf{F}^H \bar{\mathbf{A}}_D \mathbf{F}) = tr((\mathbf{R}_S \mathbf{B}_S)^H (\mathbf{R}_S \mathbf{B}_S) \mathbf{U}_F \mathbf{\Sigma}_F \mathbf{F}_M^H \cdot (\mathbf{R}_D \mathbf{B}_D)^H (\mathbf{R}_D \mathbf{B}_D) (\mathbf{U}_F \mathbf{\Sigma}_F \mathbf{V}_F^H)^H. \tag{40}$$

Utilizing the properties of the trace and SVD, (40) will be maximized if

$$(\mathbf{R}_S \mathbf{B}_S) \mathbf{U}_F = \mathbf{I}, \ (\mathbf{R}_D \mathbf{B}_D) \mathbf{V}_F = \mathbf{I}. \tag{41}$$

Then by designing $\mathbf{U}_F$ and $\mathbf{V}_F$, satisfying (41), $\mathcal{P}_{3-3}$ can be rewritten as

$$\mathcal{P}_{3-4} \quad \max_{\sigma_1, \cdots, \sigma_{\min(L_D, L_S)}} \sum_{i=1}^{\min(L_D, L_S)} \sigma_i^2 \tag{42a}$$

$$s.t. \ tr((\mathbf{U}_F \mathbf{\Sigma}_F \mathbf{V}_F^H)^H \mathbf{U}_F \mathbf{\Sigma}_F \mathbf{V}_F^H) \leq P, \tag{42b}$$

where $\Sigma_F = diag(\sigma_1, \cdots, \sigma_{\min(L_D, L_S)})$. The problem $\mathcal{P}_{3-4}$ can be solved by the MATLAB R2022b toolbox.

Having addressed the three sub-problems, the AO algorithm is detailed in Algorithm 3.

Algorithm 3: The AO Algorithm

Input: $\mathbf{R}_{S_k}$, $\mathbf{R}_{D_k}$,L_{RF}, N, $\mathcal{U}$, $\mathbf{B}_D$, $\mathbf{F}$;
Output: $\mathbf{B}_S$; $\mathbf{B}_D$
Function $f^{(i)} = \mathbb{E}\|\mathbf{G}^H\mathbf{B}_D\mathbf{F}\mathbf{B}_S^H\mathbf{H}\|_F^2$; initialize $f^{(0)} = 0$, $\mathbf{B}_S$ arbitrary matrix constructed by $\mathcal{U}$, $\mathbf{F} = \mathbf{I}$; i represents the number of iterations, initialize $i = 0$;
while $i \neq 0$ **do**
  if *i is odd* **then**
    Use the I-BS scheme in Algorithm 1 to obtain $\mathbf{B}_D$;
  else if *i is even* **then**
    Use the I-CS scheme in Algorithm 2 to obtain $\mathbf{B}_S$
  end
  Use CVX toolbox to solve $\mathcal{P}_{3-4}$ and get the parameter matrix $\mathbf{F}$;
  if $|f^{(i)} - f^{(i-1)}| > \xi$ **then**
    Set $i = i + 1$
  else if $|f^{(i)} - f^{(i-1)}| \leq \xi$ **then**
    Set $i = 0$
  end
end

3.3. Digital Pre-Coding Matrix Design in the Second Stage

Suppose that the system's IE-CSI is perfectly obtained in the second stage. Denote by $\hat{\mathbf{H}}$ and $\hat{\mathbf{G}}$ the estimations of $\mathbf{B}_S^H\mathbf{H}$ and $\mathbf{G}^H\mathbf{B}_D$, respectively. Consequently, the digital precoding matrices $\mathbf{F}_1$ and $\mathbf{F}_2$ for the UPs can be derived using the ZF strategy as

$$\mathbf{F}_1 = (\hat{\mathbf{H}})^{\dagger}\mathbf{\Gamma_1}, \mathbf{F}_2 = (\hat{\mathbf{G}})^{\dagger}\mathbf{\Gamma_2}. \tag{43}$$

where the diagonal matrices $\mathbf{\Gamma_1}$ and $\mathbf{\Gamma_2}$ are introduced to normalize the columns of $\mathbf{F}_1$ and $\mathbf{F}_2$.

After the whole transmission, the received signal of the k-th DUs is expressed as

$$\begin{aligned}\mathbf{y}_{D_k} = &\underbrace{\mathbf{g}_k^H\mathbf{B}_D\mathbf{F}_2\mathbf{P}\mathbf{F}_1\mathbf{B}_S^H\mathbf{h}_{k'}x_{S_{k'}}}_{desired\ signal} + \underbrace{\sum_{n=1,n\neq k'}^{K}\mathbf{g}_k^H\mathbf{B}_D\mathbf{F}_2\mathbf{P}\mathbf{F}_1\mathbf{B}_S^H\mathbf{h}_n x_{S_n}}_{interference} \\ &+ \underbrace{\mathbf{g}_k^H\mathbf{B}_D\mathbf{F}_2\mathbf{P}\mathbf{F}_1\mathbf{B}_S^H\mathbf{n}_R + \mathbf{n}_{D_k}}_{i.i.dAWGNnoise}.\end{aligned} \tag{44}$$

Then, the SINR for the UP (k, k') is

$$\mathbf{SINR}_{k'\to k} = \frac{\mathbb{E}\{|\mathbf{g}_k^H\mathbf{B}_D\mathbf{F}_2\mathbf{P}\mathbf{F}_1\mathbf{B}_S^H\mathbf{h}_{k'}|^2\}}{\theta_{re} + \theta_{rs} + \sigma_D^2}, \tag{45}$$

where

$$\theta_{re} = \sum_{n=1,n\neq k'}^{K}\mathbb{E}\{|\mathbf{g}_k^H\mathbf{B}_D\mathbf{F}_2\mathbf{P}\mathbf{F}_1\mathbf{B}_S^H\mathbf{h}_n|^2\}, \tag{46}$$

$$\theta_{rs} = \sigma_R^2\mathbb{E}\{\|\mathbf{g}_k^H\mathbf{B}_D\mathbf{F}_2\mathbf{P}\mathbf{F}_1\mathbf{B}_S^H\|_2^2\}. \tag{47}$$

Consequently, the ESE of the proposed TSCB scheme is

$$R = (1 - \frac{\max\{\mu_S, \mu_R\}}{T}) \sum_{k=1}^{K} \log(1 + \mathrm{SINR}_{k' \to k}). \tag{48}$$

We now analyze the convergence and computational complexity of the OA algorithm. This algorithm iteratively solves three sub-problems. For sub-problems $\mathcal{P}_{3-1}$ and $\mathcal{P}_{3-2}$, the proposed I-BS and I-CS schemes can achieve the optimal solutions. The third sub-problem also has an optimal solution using the proposed algorithm. Since all three sub-problems can achieve optimal solutions, the objective function remains non-decreasing with the iterations. Additionally, the objective function values have a Shannon bound. According to the Bolzano–Weierstrass theorem, the OA algorithm is convergent. The comparison of the complexity of different schemes is shown in Table 2. In all schemes, M is the number of relay antennas and K is the number of UPs. In the TSCB scheme, L_N is the number of alternating iterations. In the digital S-CSI scheme, τ is the computational precision, and I_R is the number of iterations. In the JSDM scheme, G represents the number of UP groups, M is the number of relay antennas, r_{total} is the number of dominant eigenvectors, and b denotes the column number of the pre-beamforming matrix.

Table 2. The comparison of the complexities of different schemes.

Scheme	Computational Complexity
I-CSI, Full-ditigal [15]	$\mathcal{O}(K^3) + \mathcal{O}(M^3)$
S-CSI, Full-ditigal [31]	$I_R\mathcal{O}(M^3 + K^3 \log \frac{1}{\tau})$
S-CSI, JSDM [33]	$\mathcal{O}\left(GMr_{total}^2 + GM^2b\right)$
S-CSI, TSCB	$\mathcal{O}(L_N L_{RF} M^2)$

4. Numerical Results

We evaluate the proposed TSCB scheme using numerical simulations and compare it with the JSDM scheme and a full-digital scheme under both I-CSI and S-CSI scenarios. The detailed simulation parameters are shown in Table 3. In the table, the energy threshold ξ is a critical parameter that balances the pilot overhead and estimation accuracy. A too-low ξ degrades ESE due to increased pilot overhead, while a high ξ reduces ESE by filtering out critical CSI components via over-sparsification.

Table 3. The detailed simulation parameters.

Description	Symbol	Value/Range
Number of RS Antennas	M	64
Number of UPs	K	8∼25
Angle Spread	$\Delta_{S_k}, \Delta_{D_k}$	5°
Number of RF Chains	L_{RF}	16∼32
Minimum NOP Constraint	N	6∼20
Covers low-, medium-, and high-SNR Scenarios	SNR	−15∼15 dB
Correlation between a UP and a Codeword	ξ	10^{-2}
Number of Coherent Time Transmission Symbols	T	100

Figure 3 illustrates the ESEs of all schemes across varying SNRs, with $K = 5$ and $K = 8$. The TSCB scheme's performance increases monotonically with SNR, and its growth slope is

steeper in the low SNR range and flattens in the high SNR range. At SNR = 20 dB, the TSCB scheme achieves a 13.6% gain over the JSDM scheme at $K = 8$. More importantly, the TSCB scheme outperforms all other schemes. Table 4 is used to better show the performance of all schemes. Figure 4 shows the ESEs of all schemes across varying SNRs with $N = 10, 15, 20$. The ESEs of all the schemes increase monotonically with SNR, while the proposed TSCB scheme consistently outperforms other schemes. Moreover, the ESEs increase with the increasing number of pilots N. The TSCB scheme outperforms the JSDM by 9.1% at $N = 15$.

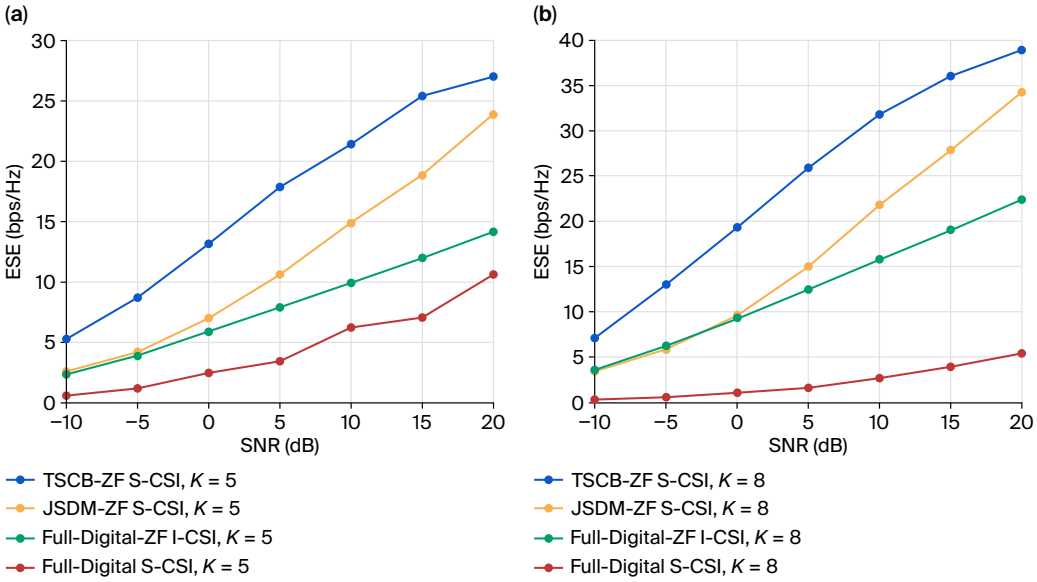


Figure 3. ESE vs. SNR ($L_{RF} = 32$, $N = 15$). (**a**) $K = 5$, (**b**) $K = 8$.

Table 4. The ESE (in bps/Hz) of the schemes with different SNRs at $L_{RF} = 20$, $N = 20$, $K = 8$.

Scheme	SNR						
	−10	**5**	**0**	**5**	**10**	**15**	**20**
S-CSI, TSCB	7.121	13.031	19.324	25.911	31.810	36.052	38.937
S-CSI, JSDM	3.418	5.863	9.595	14.986	21.794	27.837	34.272
I-CSI, Digital	3.852	6.228	9.220	12.459	15.750	18.986	22.393
S-CSI, Digital	3.852	6.228	9.220	12.459	15.750	18.986	22.393

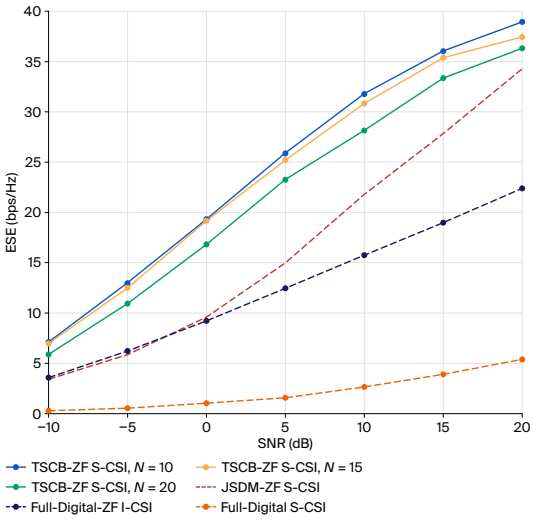


Figure 4. ESE vs. SNR. ($K = 8$, $L_{RF} = 32$, $N = 10$, $N = 15$, $N = 20$).

Figure 5 shows that, with increases in K, the ESEs of the TSCB and JSDM schemes first increase and then decrease, where the decrease is mainly due to the multi-user interference. The TSCB scheme maintains a consistent advantage over all other schemes. Figure 6 depicts the ESEs of all schemes under different L_{RF}. The ESE of the proposed scheme first increases and then decreases with the increasing L_{RF}. The proposed scheme also outperforms other schemes.

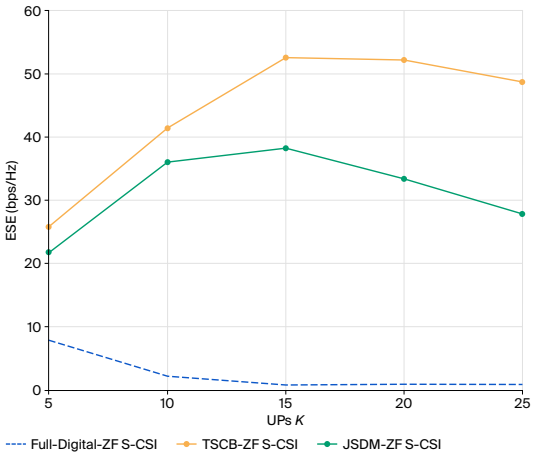


Figure 5. ESE vs. UPs ($N = 15$, SNR $= 20$, $L_{RF} = 32$).

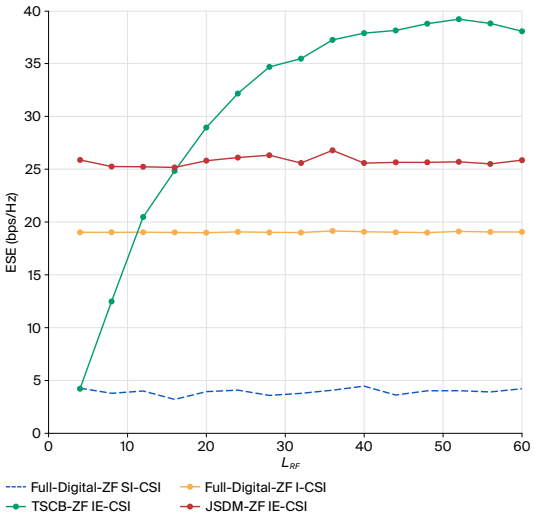


Figure 6. ESE vs. RF chains ($K = 8$, $N = 15$, SNR $= 20$).

The NOPs of the proposed TSCB scheme and the benchmark JSDM scheme at $N = 15$ are shown in Table 5. The NOPs of both schemes are highly reduced compared to the numbers of UPs and RSs.The JSDM scheme exhibits more significant NOP growth as the number of UPs increases. The NOP of the TSCB scheme is primarily determined by the number of beams.

Table 5. The NOP of the schemes at $L_{RF} = 32$, $N = 15$.

Scheme	TSCB ($K = 8$)	JSDMT ($K = 8$)	TSCB ($K = 20$)	JSDMT ($K = 20$)
NOP	11	9	12	15

5. Conclusions

In this paper, we have proposed a novel TSCB scheme for the FDD massive MIMO relay system. In the first stage, analog pre-combining and pre-beamforming matrices are

co-designed using S-CSI. Subsequently, the digital precoding matrix is designed based on the estimated IE-CSI in the second stage. The TSCB scheme reduces the dimension of the IE-CSI, greatly reducing pilot overhead and enhancing system performance. Simulation results demonstrate the superiority of the proposed TSCB scheme. In the future, we will extend the TSCB scheme to the multi-scattering cluster environments.

Author Contributions: Conceptualization, D.G., T.G. and H.L.; methodology, D.G., T.G. and H.L.; software, D.G. and H.L.; validation, D.G., Y.S. and T.G.; formal analysis, D.G. and Y.S.; investigation, D.G. and H.L.; resources, Y.S.; writing—original draft preparation, D.G.; writing—review and editing, D.G., Y.S., H.L. and T.G.; supervision, Y.S. and H.L.; project administration, Y.S. and T.G.; funding acquisition, Y.S. All authors have read and agreed to the published version of the manuscript.

Funding: This work was supported in part by the Natural Science Foundation of China under Grant 62371249 and 62101282.

Informed Consent Statement: Not applicable.

Data Availability Statement: Dataset available on request from the authors.

Conflicts of Interest: The authors declare no conflicts of interest.

Abbreviations

The following abbreviations are used in this manuscript:

AWGN	Additive White Gaussian Noise
AO	Alternating Optimization
BC	Broadcast Channel
I-BS	Iterative Beamforming Selection
I-CS	Iterative Combining Selection
DFT	Discrete Fourier Transform
ESE	Effective Spectral Efficiency
FDD	Frequency Division Duplexing
I-CSI	Instantaneous Channel State Information
IE-CSI	Equivalent Instantaneous Channel State Information
i.i.d.	independently and identically distributed
JSDM	Joint Spatial Division and Multiplexing
MAC	Multiple Access Channel
MIMO	Multiple-Input Multiple-Output
NOP	Number of Orthogonal Pilots
RF	Radio Frequency
RS	Relay Station
S-CSI	Statistical Channel State Information
SE	Spectral Efficiency
SU	Source User
TDD	Time Division Duplex
TSB	Two-stage Beamforming
TSCBUS	Two-stage Combining and Beamforming with User-pair Scheduling
ULA	Uniform Linear Arrays

References

1. Li, J.; Li, T.; Ren, J.; Chao, H. Enjoy the benefit of network coding: Combat pollution attacks in 5G multihop networks. *Wirel. Commun. Mob. Comput.* **2018**, *1*, 3473910. [CrossRef]
2. Agiwal, M.; Roy, A.; Saxena, N. Next generation 5G wireless networks: A comprehensive survey. *IEEE Commun. Surv. Tutor.* **2016**, *18*, 1617–1655. [CrossRef]
3. Liu, X. Low-complexity unsupervised learning-based hybrid precoding for massive MIMO systems. *IET Commun.* **2023**, *17*, 1773–1779. [CrossRef]

4. Chowdhury, M.; Shahjalal, M.; Ahmed, S.; Jang, Y. 6G wireless communication systems: Applications, requirements, technologies, challenges, and research directions. *IEEE Open J. Commun. Soc.* **2020**, *1*, 957–975. [CrossRef]
5. Jiang, X.; Li, P.; Li, B.; Zou, Y.; Wang, R. Secrecy performance of transmit antenna selection for underlay MIMO cognitive radio relay networks with energy harvesting. *IET Commun.* **2022**, *16*, 227–245. [CrossRef]
6. Fazeli, S.; Akhlaghi, S. Null-space beamforming strategy for secrecy rate balancing of two-way MIMO relay networks. *IET Commun.* **2023**, *17*, 2080–2096. [CrossRef]
7. Khodeir, M.; Al-Mistarthi, M.; Ibrahem, L. Performance evaluation of cognitive relay networks for end-user mobile over mixed realistic channels. *IET Commun.* **2023**, *17*, 228–245. [CrossRef]
8. Du, J.; Ye, S.; Chen, Y.; Guan, Y. Joint channel estimation techniques for multi-user massive MIMO relay networks. In Proceedings of the 2020 IEEE 20th International Conference on Communication Technology (ICCT), Nanning, China, 28–31 October 2020; pp. 29–33.
9. Peng, Z.; Wang, S.; Pan, C.; Chen, X.; Cheng, J.; Hanzo, L. Multi-pair two-way massive MIMO DF relaying over Rician fading channels under imperfect CSI. *IEEE Wirel. Commun. Lett.* **2021**, *11*, 225–229. [CrossRef]
10. Zhang, Y.; Zhang, H.; Zhou, X.; Yuan, D.; Cao, Y. Relay assisted Max-SINR transceiver optimization design for MIMO interference channels. *IEEE Trans. Veh. Technol.* **2022**, *72*, 2066–2081. [CrossRef]
11. Alahmadi, A.; Liang, Y.; Tian, R.; Ren, J.; Li, T. Blocking probability analysis for relay-assisted OFDMA networks using stochastic geometry. In Proceedings of the 2019 International Conference on Computing, Networking and Communications (ICNC), Honolulu, HI, USA, 18–21 February 2019; pp. 509–514.
12. Suraweera, H.A.; Ngo, H.Q.; Duong, T.Q.; Yuen, C.; Larsson, E.G. Multi-pair amplify-and-forward relaying with very large antenna arrays. In Proceedings of the 2013 IEEE International Conference on Communications (ICC), Budapest, Hungary, 9–13 June 2013; pp. 4635–4640.
13. Chen, Y.; Liu, C.; Wang, H.; Zhu, W.P. Performance analysis for multi-pair massive MIMO AF relay networks with ZF processing. In Proceedings of the GLOBECOM 2017-2017 IEEE Global Communications Conference, Singapore, 4–8 December 2017; pp. 1–6.
14. Rahimi, R.; Shahbazpanahi, S. A two-way network beamforming approach based on total power minimization with symmetric relay beamforming matrices. *IEEE Access* **2017**, *5*, 12458–12474. [CrossRef]
15. Chen, X.; Peng, Z.; Pan, C.; Ren, H.; Wang, L.C. Performance analysis and power allocation of multi-pair two-way massive MIMO full-duplex DF relaying systems under Rician fading channels. *IEEE Trans. Veh. Technol.* **2022**, *72*, 1955–1971. [CrossRef]
16. Rezaei, A.; Falahati, A.; Zargari, S. Energy efficient multi-Way massive MIMO AF relaying with imperfect CSI and optimal power allocation. *Wirel. Pers. Commun.* **2023**, *132*, 1681–1702. [CrossRef]
17. Xu, M.; Mao, M.; Feng, Y.; Li, T.; Shi, R.; He, Y. Beamforming design for max-min SINR in RIS-based hybrid relaying. *IET Commun.* **2023**, *17*, 1220–1227. [CrossRef]
18. Rong, Y.; Khandaker, M.R.; Xiang, Y. Channel estimation of dual-hop MIMO relay system via parallel factor analysis. *IEEE Trans. Wirel. Commun.* **2012**, *11*, 2224–2233. [CrossRef]
19. Chen, H.; Lam, W.H. Training-based two-step channel estimation in two-Way MIMO relay systems. *IEEE Trans. Veh. Technol.* **2017**, *67*, 2193–2205. [CrossRef]
20. Ngo, H.Q.; Suraweera, H.A.; Matthaiou, M.; Larsson, E.G. Multipair full-duplex relaying with massive arrays and linear processing. *IEEE J. Sel. Areas Commun.* **2014**, *32*, 1721–1737. [CrossRef]
21. Xu, W.; Liu, J.; Jin, S.; Dong, X. Spectral and energy efficiency of multi-pair massive MIMO relay network with hybrid processing. *IEEE Trans. Commun.* **2017**, *65*, 3794–3809. [CrossRef]
22. Chauhan, A.S.; Sharma, E.; Budhiraja, R. Hybrid block diagonalization for massive MIMO two-way half-duplex AF hybrid relay. In Proceedings of the 2018 International Conference on Signal Processing and Communications (SPCOM), Bangalore, India, 16–19 July 2018; pp. 367–371.
23. Fozooni, M.; Ngo, H.Q.; Matthaiou, M.; Jin, S.; Alexandropoulos, G.C. Hybrid processing design for multipair massive MIMO relaying with channel spatial correlation. *IEEE Trans. Commun.* **2018**, *67*, 107–123. [CrossRef]
24. Spectral and energy efficiency for large-scale multiple-input-multiple-output two-Way hybrid relaying with multi-pair users under imperfect channel state information. *IEEE Access* **2021**, *9*, 142837–142856. [CrossRef]
25. Qian, J.; Masouros, C. Multipair relaying with space-constrained large-scale MIMO arrays: Spectral and energy efficiency analysis with incomplete CSI. *IEEE Open J. Commun. Soc.* **2021**, *2*, 2357–2371. [CrossRef]
26. Long, H.; Xiang, W.; Zhang, L.; Huang, L. MMSE-based secure precoding in two-way relaying systems. *IET Commun.* **2020**, *14*, 3813–3819. [CrossRef]
27. Jiang, Z.; Molisch, A.F.; Caire, G.; Niu, Z. Achievable rates of FDD massive MIMO systems with spatial channel correlation. *IEEE Trans. Wirel. Commun.* **2015**, *14*, 2868–2882. [CrossRef]
28. Li, S.; Xing, C.; Fei, Z.; Kuang, J. Robust two-way amplify-and-forward MIMO relay beamforming with non-reciprocal and reciprocal CSI. In Proceedings of the 7th International Conference on Communications and Networking in China, Kunming, China, 8–10 August 2012; pp. 343–347.

29. Dutta, B.; Budhiraja, R.; Koilpillai, R.D.; Hanzo, L. Analysis of quantized MRC-MRT precoder for FDD massive MIMO two-Way AF relaying. *IEEE Trans. Commun.* **2018**, *67*, 988–1003. [CrossRef]
30. Rezvani, S.M.; Keshavarz, H. Two-way MIMO relay beamforming scheme for sum-rate maximization approach based on second-order statistics. In Proceedings of the 2016 24th Iranian Conference on Electrical Engineering (ICEE), Shiraz, Iran, 10–12 May 2016; pp. 29–33.
31. Zhang, R.; Leung, S.H.; Luo, Z.; Wang, H. Precoding design for correlated MIMO-AF relay networks with statistical channel state information. *IEEE Trans. Signal Process.* **2018**, *66*, 5902–5916. [CrossRef]
32. Dilli, R. Hybrid beamforming in 5G nr networks using multi user massive MIMO at FR2 frequency bands. *Wirel. Pers. Commun.* **2022**, *127*, 3677–3709. [CrossRef]
33. Adhikary, A.; Nam, J.; Ahn, J.Y.; Caire, G. Joint spatial division and multiplexing—The large-scale array regime. *IEEE Trans. Inf. Theory* **2013**, *59*, 6441–6463. [CrossRef]
34. Song, Y.C.; Liu, C.; Liu, Y.L.; Cheng, N.; Huang, Y.M.; Shen, X.M. Joint spatial division and multiplexing in massive MIMO: A neighbor-based approach. *IEEE Trans. Wirel. Commun.* **2020**, *19*, 7392–7406. [CrossRef]
35. Song, Y.C.; Liu, C.; Zhang, W.Y.; Liu, Y.L.; Zhou, H.B.; Shen, X.M. Two-stage beamforming in massive MIMO: A combinatorial multi-armed bandit-based approach. *IEEE Trans. Veh. Technol.* **2023**, *72*, 6794–6799. [CrossRef]

Disclaimer/Publisher's Note: The statements, opinions and data contained in all publications are solely those of the individual author(s) and contributor(s) and not of MDPI and/or the editor(s). MDPI and/or the editor(s) disclaim responsibility for any injury to people or property resulting from any ideas, methods, instructions or products referred to in the content.